Materials and Structures (2024) 57:47
https://doi.org/10.1617/s11527-024-02315-z

ORIGINAL ARTICLE

Impact of supplementary cementitious materials on the solid–liquid equilibrium curve of calcium in cement hydrates

Ming Zhang · Peicheng Shen · Dujian Zou · Tiejun Liu · Shanshan Qin · Ao Zhou · Ye Li

Received: 16 June 2023 / Accepted: 1 February 2024 / Published online: 12 March 2024
© The Author(s), under exclusive licence to RILEM 2024

Abstract The leaching of calcium in cement hydrates, particularly in harsh environments, significantly affects the durability of cement-based materials. Understanding the solid–liquid equilibrium of calcium is essential to elucidate the leaching mechanism and leachability for developing accurate degradation models of cementitious materials under chloride exposure. In this study, the effects of different types and proportions of supplementary cementitious materials (SCMs) on the calcium leaching process were investigated. This was achieved by simulating pore solutions at various leaching degrees. Key parameters of the equilibrium curves were extracted and analyzed at different leaching stages. Additionally, a functional relationship between these parameters and the proportions of various SCMs was established. The leachability was assessed by comparing the saturated concentration of calcium ions, the total concentration of solid-phase calcium, and the relative content of calcium hydroxide (CH) and calcium silicate hydrate (C–S–H). It was found that composite binder pastes containing 50% slag demonstrated the best performance in terms of calcium leaching resistance. This research provides valuable insights for the design of anti-leaching cementitious materials and contributes to the development of precise deterioration models for concrete exposed to aggressive environments.

Keywords Calcium leaching · Solid–liquid equilibrium curve · Supplementary cementitious materials · Chloride attack · Concrete durability

1 Introduction

Chloride-induced deterioration poses a significant threat to the integrity of marine concrete structures. Chloride ions infiltrate the protective layers of concrete, reaching the reinforcing steel surfaces, and consequently disrupting the steel's passivating film. This leads to corrosion, a major global challenge for concrete structures [1]. Additionally, concrete exposed to complex marine environments over extended periods is prone to calcium leaching in its surface layer. This is attributed to the concentration gradients between external seawater calcium ions and those in the pore solutions [2]. Calcium leaching not only impairs the

M. Zhang · P. Shen · D. Zou (✉) · T. Liu · A. Zhou · Y. Li
School of Civil and Environmental Engineering, Harbin Institute of Technology, Shenzhen, Shenzhen 518055, People's Republic of China
e-mail: zoudujian@163.com

M. Zhang · P. Shen · D. Zou · T. Liu · A. Zhou · Y. Li
Guangdong Provincial Key Laboratory of Intelligent and Resilient Structures for Civil Engineering, Harbin Institute of Technology, Shenzhen, Shenzhen 518055, People's Republic of China

S. Qin
School of Construction Engineering, Shenzhen Polytechnic University, Shenzhen 518055, People's Republic of China

mechanical integrity of the concrete matrix but also modifies the pore structure. Such alterations facilitate the ingress of aggressive ions, thereby exacerbating durability issues [3].

In contrast to the slower calcium leaching process observed in pure water, the presence of chloride ions in the marine environment accelerates the leaching process due to the coupled action [4]. This leaching process undermines the concrete's pore structure, expediting the penetration of harmful ions and accelerating steel corrosion. Concurrently, chloride attack leads to the expansion of steel corrosion, creating cracks in the concrete. These cracks further expedite calcium ion transport, thus intensifying the leaching process in the concrete. According to standards such as ACI 318-19 [5], BS EN 206:2013 [6], and GB/T 50476-2019 [7], the critical chloride threshold for steel reinforcement is a crucial factor in determining the limit states of corrosion initiation. However, the interplay between calcium leaching and chloride ion transport challenges the precision of quantitative durability design for concrete structures in chloride-laden environments.

As global priorities shift towards green, low-carbon, and sustainable development, the conventional, energy-intensive, and high-carbon-emission cement materials are increasingly being substituted with various supplementary cementitious materials (SCMs) [8]. The utilization of SCMs offers multiple advantages, including the reduction of CO_2 emissions, lowered production costs, and the mitigation of environmental pollution [9]. Moreover, SCMs contribute to altering the hydrate composition and microstructure of concrete, thereby enhancing its mechanical properties and durability [10]. The impact of SCMs on the leaching performance of composite binder pastes has received extensive research attention, owing to the variance in particle size, shape, physical effects, and chemical activity of different SCMs. Studies have explored a range of SCMs, such as chopped basalt fibers [11], nano silica [12], CO_2-treated municipal solid waste incineration fly ash [13], activated paper sludge [14], silica fume [15], titanium dioxide [16], and limestone [17].

Qiao et al. [18] examined the calcium leaching behavior of cement pastes under $MgCl_2$ attack and showed that the addition of fly ash, reducing the CH content, could inhibit the decline in flexural strength. Zuo et al. [19] performed accelerated leaching tests on composite binder pastes comprising pure cement, cement-fly ash binary systems, and cement-fly ash-slag ternary systems under NH_4NO_3 attack. These studies [15, 20–23] indicate that SCMs can improve the leaching resistance of cementitious materials by consuming CH and refining pore sizes, which helps resist the infiltration of aggressive ions. Notably, fly ash was found to increase the leaching depth while reducing the overall degree of calcium leaching. Conversely, the addition of slag was observed to enhance paste compactness and optimize microstructure, thereby reducing the leaching depth. However, it is important to note that a higher proportion of SCMs does not necessarily enhance leaching resistance. Phung et al. [24] demonstrated that an increased water-to-binder ratio and higher limestone contents could accelerate calcium leaching. In addition to exploring the leaching properties of cementitious materials through accelerated experiments, Zhang et al. [25] investigated the reinforcing mechanisms of SCMs, epoxy resin, and graphene oxide in enhancing the erosion resistance of concrete. This was conducted through molecular dynamics simulations at the nano-scale, providing theoretical backing for the development of anti-erosion concrete materials.

Extensive theoretical analyses and numerical models are currently being developed to quantify the behavior of calcium leaching [26, 27]. Models for calcium dissolution–diffusion in various solutions, such as pure water [28], NH_4NO_3 [29], and Na_2SO_4 [30], have been established. Additionally, the impact of calcium leaching on porosity and diffusion coefficients is considered in some concrete deterioration models [31–34]. The calcium leaching process is commonly quantified in these models using the solid–liquid equilibrium curve [35], which illustrates the relationship between the dissolution of solid-phase calcium in cement hydrates and the diffusion of liquid-phase calcium in pore solutions [36]. Gérard et al. [37] formulated a solid–liquid equilibrium equation that categorizes the calcium leaching process into three stages: rapid CH dissolution, gradual C–S–H leaching, and rapid C–S–H leaching [28, 38]. Subsequent studies by Wan et al. [39, 40], Zou et al. [30], and Tang et al. [41] examined the variations in solid–liquid equilibrium curves across different aggressive solution types and concentrations. Experimental investigations by Yokozeki et al. [42] and Gawin et al. [43] analyzed the equilibrium

curve in deionized water under varying temperatures. These studies highlight how the concentration, type, and temperature of aggressive solutions can influence leaching stages and key equilibrium curve parameters, thereby impacting the accuracy of concrete deterioration models that consider calcium leaching in aggressive environments [44].

Furthermore, the solid–liquid equilibrium curve has been utilized to describe calcium leaching in cementitious materials containing SCMs. Gérard et al. [45] applied it to silica fume–cement composite pastes, while Phung et al. [46] used it to study the effects of limestone on the leaching kinetics of cement paste. Jain et al. [47] investigated calcium leaching in cement pastes modified with high-alkali fine glass powder, silica fume, and fly ash. The equilibrium curve has also been employed to simulate calcium leaching kinetics in cement asphalt paste [48] and early carbonated concrete [49]. Based on these findings, employing the solid–liquid equilibrium curve to examine calcium leaching in composite binder pastes with varying types and proportions of SCMs appears justified.

However, a gap remains in defining reliable key parameters of equilibrium curves for deterioration models of composite binder pastes under chloride attack. Furthermore, the resistance of composite binder systems to calcium leaching varies with the type and proportion of SCMs [50]. While some accelerated leaching experiments have sought to identify optimal SCM types and proportions for calcium leaching resistance by examining factors such as leaching depth and microstructure [51, 52], research focusing on solid–liquid equilibrium curves remains limited. In this study, we investigate the influence of SCMs on solid–liquid equilibrium curves to establish a functional relationship between key parameters and SCM proportions. This approach aims to guide the development of concrete deterioration models that account for calcium leaching under chloride attack. Additionally, we compare parameters like the saturated concentration of calcium ions, relative content of CH and C–S–H, and total solid-phase calcium to determine the most effective SCM type and proportion for optimal leaching resistance.

2 Materials and methods

2.1 Materials

The study utilized various cementitious materials, including ordinary Portland cement (P.O 42.5R), silica fume (SiO_2 content of at least 95%), type I fly ash, and granulated blast furnace slag (S95). The chemical composition, density, and specific surface area of these materials are detailed in Table 1. For the experimental solvent, deionized water was used, adhering to the national standard GB6682-2008. This water was colorless, tasteless, and non-corrosive. Sodium chloride (NaCl), with a purity of at least 99.5%, was employed in line with the national standard GB/T 1266-2006.

2.2 Experimental design

The experimental design adhered to the maximum SCM proportion stipulated in the standard DB11/T 1029–2021. The proportions for fly ash, slag, and silica fume in the composite binder pastes were set at

Table 1 Chemical composition and physical characteristics of cementitious materials

Cementitious materials		Cement	Slag	Silica fume	Fly ash
Chemical composition (wt.%)	CaO	62.79	41.71	0.17	1.94
	SiO_2	20.66	29.14	96.80	54.66
	Al_2O_3	5.56	16.46	0.00	35.14
	Fe_2O_3	3.93	0.29	0.08	3.11
	MgO	2.39	7.92	0.35	0.88
	SO_3	3.02	0.00	1.86	0.64
	K_2O	0.85	0.39	0.38	1.35
	Na_2O	0.13	0.58	0.16	0.41
Specific area (m^2/kg)		351	429	21,000	430
Density (kg/m^3)		3150	2907	2270	2151

a maximum of 30, 55, and 10%, respectively. Consequently, silica fume proportions were established at 5, 10, and 15%, while fly ash was tested at 10, 20, and 30% dosages. For slag, considering its potential water hardness and maximum permissible dosage of 55%, five groups were created with 10, 20, 30, 40, and 50% dosage levels. The water-to-binder ratio was maintained at 0.4. A 3% NaCl solution was used as the aggressive solution, prepared based on the mass fraction of chloride ions in seawater, excluding the influence of other aggressive ions [53–56]. Table 2 details the specific experimental conditions.

2.3 Experimental process

Each point on the solid–liquid equilibrium curve represents the dissolution–diffusion equilibrium state between the solid-phase calcium in cement hydrates and the liquid-phase calcium ions in the pore solution. This equilibrium state at various leaching stages was simulated by adjusting the ratio of aggressive solutions to cement pastes, as detailed in Table 3. The experimental procedure was divided into three stages: dissolution experiment, determination of solid and liquid-phases calcium, and fitting of leaching curves (refer to Fig. 1 for a schematic representation). Initially, specimens cured for over 3 months were dried at 40 °C to remove surface moisture. Subsequently, the non-carbonized portion was ground into powder and sieved through a 200-mesh screen. Based on the proportions outlined in Table 3, pastes and solutions were thoroughly mixed using a magnetic stirrer for seven days to achieve dissolution equilibrium. Following dissolution, the solid and liquid phases were separated through vacuum pump filtration using a microporous filter membrane (0.45 μm). The calcium content in the liquid phase was determined using the EDTA titration method [57]. To ensure accuracy, each equilibrium point was repeated three times, aiming for a relative error of less than 3%. The calcium content in the solid phase was calculated by subtracting the measured liquid-phase calcium from the initial total calcium concentration.

Table 2 Design of experimental conditions

ID	Composite binder paste	Aggressive solution	SCMs proportion
PO-w	Pure cement paste	Deionized water	–
PO-0		3% NaCl	
SF-5	Silica fme–cement	3% NaCl	5%
SF-10			10%
SF-15			15%
FA-10	Fly ash–cement	3% NaCl	10%
FA-20			20%
FA-30			30%
SL-10	Slag–cement	3% NaCl	10%
SL-20			20%
SL-30			30%
SL-40			40%
SL-50			50%

Table 3 Proportion of aggressive solutions and cement pastes for different leaching stages

Experimental ID	Paste powder (g)	Solution volume (mL)	Experimental ID	Paste powder (g)	Solution volume (mL)
1	12	250	8	1	250
2	10	250	9	1	500
3	8	250	10	1	750
4	6	250	11	1	1000
5	4	250	12	1	1500
6	2	250	13	1	2000
7	1.5	250	14	1	3000

2.4 Determination of solid–liquid equilibrium curve parameters

The mathematical representation of the solid–liquid equilibrium curve is shown in Eq. (1). The calcium concentrations in cement hydrates and pore solutions are denoted as C_{solid} and C_{liquid}, respectively. x_1 represents the concentration of calcium ions in the pore solution at the onset of rapid C–S–H dissolution; x_2 is the concentration of calcium ions at the onset of slow C–S–H dissolution when CH is fully dissolved. C_{satu} represents the saturated calcium ion concentration in the pore solution. These parameters (x_1, x_2, and C_{satu}) are critical in defining the leaching curve and are influenced by external aggressive solutions.

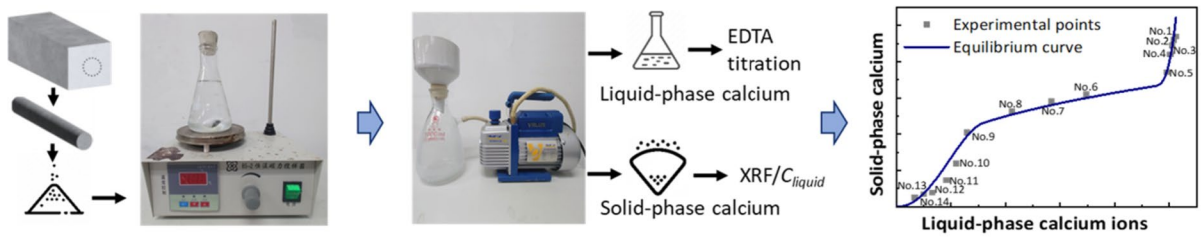

Fig. 1 Experimental procedure for determining the solid–liquid equilibrium curve

$$C_{\text{solid}} = \begin{cases} \left(\dfrac{-2}{x_1^3}C_{\text{liquid}}^3 + \dfrac{3}{x_1^2}C_{\text{liquid}}^2\right)\left[C_{\text{CSH0}}\left(\dfrac{C_{\text{liquid}}}{C_{\text{satu}}}\right)^{1/3}\right] & 0 \le C_{\text{liquid}} \le x_1 \\ \left[C_{\text{CSH0}}\left(\dfrac{C_{\text{liquid}}}{C_{\text{satu}}}\right)^{1/3}\right] & x_1 \le C_{\text{liquid}} \le x_2 \\ \left[C_{\text{CSH0}}\left(\dfrac{C_{\text{liquid}}}{C_{\text{satu}}}\right)^{1/3}\right] + \dfrac{C_{\text{CH0}}}{(C_{\text{satu}} - x_2)^3}(C_{\text{liquid}} - x_2)^3 & x_2 \le C_{\text{liquid}} \le C_{\text{satu}} \end{cases} \quad (1)$$

where C_{CSH0} and C_{CH0} represent the initial calcium concentration in the C–S–H and CH of composite binder pastes, respectively, which are related to the material composition of pastes. They can be quantitatively calculated from their oxide composition using Bogue's equations or measured experimentally via techniques such as quantitative X-ray diffraction, microscopy, and liquid extraction [58].

It should be noted that the calculation of C_{CSH0} and C_{CH0} in composite binder pastes differs from that in pure cement pastes due to the pozzolanic properties of SCMs. Specifically, the SiO_2 in silica fume or fly ash reacts only with CH in cement hydrates. In contrast, the CaO in slag exhibits hardening properties upon excitation of CH in cement hydrates. Furthermore, SiO_2 and Al_2O_3 in slag undergo secondary hydration with CH to form C–(A)–S–H. In this study, the calcium to silica ratio in C–S–H generated by cement hydration is 1.7 [47], while for the hydration by silica fume or fly ash, it is 1.1 [59]. To enhance comparability in leaching resistance among different composite cement pastes, this study assumes that the leaching properties of C–S–H and C–A–S–H are similar, and the calcium–silicon ratio of C–S–H and C–A–S–H are averaged to an equilibrated.

Thus, C_{CSH0} and C_{CH0} are calculated separately for slag cement and silica fume or fly ash cement. For silica fume or fly ash cement pastes, the C–S–H and CH generated by cement hydration ($C_{\text{CSH}}^{\text{cement}}$, $C_{\text{CH}}^{\text{cement}}$) are expressed as Eqs. (2) and (3). The amount of CH consumed ($C_{\text{CH*}}^{\text{SF/FA}}$) and the C–S–H generated ($C_{\text{CSH}}^{\text{SF/FA}}$) by silica fume or fly ash are calculated using Eqs. (4) and (5).

$$C_{\text{CSH}}^{\text{cement}} = \left(1.7 \times f_{C_3S}/228 + 1.7 \times f_{C_2S}/172\right) \times \rho \times m^{\text{cement}}/(1 + w/c) \times \alpha \times 10^6 \quad (2)$$

$$C_{\text{CH}}^{\text{cement}} = \left(1.3 \times f_{C_3S}/228 + 0.3 \times f_{C_2S}/172\right) \times \rho \times m^{\text{cement}}/(1 + w/c) \times \alpha \times 10^6 \quad (3)$$

$$C_{CH*}^{SF/FA} = -1.1 \times SiO_2^{SF/FA} / M_{SiO_2} \times m^{SF/FA} \times \rho/(1 + w/c) \times \alpha^{SF/FA} \times 10^6 \quad (4)$$

$$C_{CSH}^{SF/FA} = 1.1 \times SiO_2^{SF/FA} / M_{SiO_2} \times m^{SF/FA} \times \rho/(1 + w/c) \times \alpha^{SF/FA} \times 10^6 \quad (5)$$

$$\alpha = 0.239 + 0.745\tanh\left[3.62 \times \left(w/\left(c + \alpha^{SF/FA} m^{SF/FA}\right) - 0.095\right)\right] \quad (6)$$

where α and $\alpha^{SF/FA}$ are the hydration degree of pure cement paste and silica fume (or fly ash), respectively; $SiO_2^{SF/FA}$ and M_{SiO_2} are the mass fraction and molar mass of SiO_2 in the silica fume or fly ash; m^{cement} and $m^{SF/FA}$ are the masses of cement and silica fume or fly ash in the composite binder paste, respectively; f_{C_3S} and f_{C_2S} can be calculated by Bogue's equations; ρ is the density of composite binder pastes. For slag–cement hydration, stoichiometric models [58] are used as shown in Eqs. (7) to (16).

$$n_{C_3S}^{cement} = \left(f_{C_3S} / M_{C_3S}\right) \times m^{cement} \times \alpha \quad (7)$$

$$n_{C_2S}^{cement} = \left(f_{C_2S} / M_{C_2S}\right) \times m^{cement} \times \alpha \quad (8)$$

$$n_{CH}^{cement} = 1.3 n_{C_3S}^{cement} + 0.3 n_{C_2S}^{cement} \quad (9)$$

$$n_{CaO}^{SL} = m^{SL} \times \alpha^{SL} \times \left(\frac{CaO^{SL}}{M_{CaO}} - 2 \times \frac{SO_2^{SL}}{M_{SO_2}}\right) \quad (10)$$

$$n_{Al_2O_3}^{SL} = m^{SL} \times \alpha^{SL} \times \left(\frac{Al_2O_3^{SL}}{M_{Al_2O_3}} - \frac{MgO^{SL}}{5 \times M_{MgO}} - \frac{SO_2^{SL}}{3 \times M_{SO_2}}\right) \quad (11)$$

$$n_{Al_2O_3}^{SL} = m^{SL} \times \alpha^{SL} \times \left(\frac{Al_2O_3^{SL}}{M_{Al_2O_3}} - \frac{MgO^{SL}}{5 \times M_{MgO}} - \frac{SO_2^{SL}}{3 \times M_{SO_2}}\right) \quad (12)$$

$$p = \frac{1.7 n_{SiO_2}^{SL} - n_{CaO}^{SL}}{n_{CH}^{cement} + 1.7 n_{SiO_2}^{SL} - n_{CaO}^{SL}} \quad (13)$$

$$\lambda_{Ca/Si} = \frac{1.7\left(n_{C_3S}^{cement} + n_{C_2S}^{cement}\right) + n_{CaO}^{SL} + p n_{CH}^{cement} + 0.85 n_{SiO_2}^{SL} - 4 n_{Al_2O_3}^{SL}}{1.36 n_{SiO_2}^{SL} + n_{C_3S}^{cement} + n_{C_2S}^{cement}} \quad (14)$$

$$C_{CH*}^{SL} = p \times n_{CH}^{cement} \times \rho/(1 + w/c) \times 10^6 \quad (15)$$

$$C_{CSH}^{SL} = n_{SiO_2}^{SL} \times \lambda_{Ca/Si} \times \rho/(1 + w/c) \times 10^6 \quad (16)$$

where M_i and n_i^j represent the molar mass and moles of the phase i in j (cement or slag); p is the proportion of the consumed CH to the total amount produced; $\lambda_{Ca/Si}$ is the averaged calcium-silica ratio; α^{SL} is the hydration degree of slag. Combining the analyses above, C_{CSH0} and C_{CH0} in composite binder paste before calcium leaching can be calculated as:

$$C_{CH0} = C_{CH}^{cement} + C_{CH*}^{SF/FA/SL} \quad (17)$$

$$C_{CSH0} = C_{CSH}^{cement} + C_{CSH}^{SF/FA/SL} \quad (18)$$

3 Results and discussion

3.1 Analysis of the solid–liquid equilibrium curve

3.1.1 Solid–liquid equilibrium curves of pure cement pastes

The solid–liquid equilibrium curves for pure cement pastes in 3% NaCl and deionized water are depicted in Fig. 2. These curves illustrate that the calcium leaching process in NaCl solution follows a similar three-stage pattern as in deionized water, characterized by rapid dissolution of CH, followed by slow decalcification of C–S–H, and then a rapid decalcification of C–S–H. Table 4 presents the fitting parameters of these equilibrium curves, derived from experimental data.

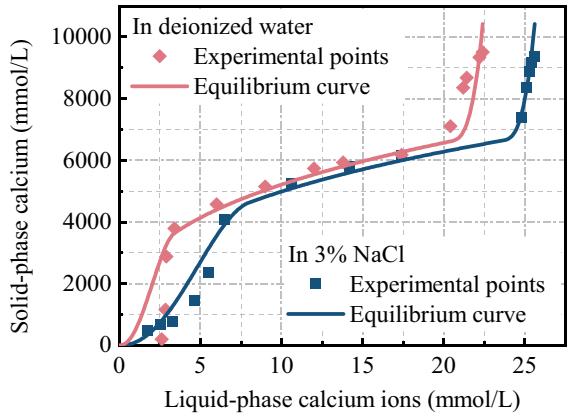

Fig. 2 Solid–liquid equilibrium curves of pure cement pastes

Table 4 Fitting parameters of equilibrium curves in the pure cement paste group

Fitting parameters	x_1 (mol/m^3)	x_2 (mol/m^3)	C_{satu} (mol/m^3)	C_{CSH0} (mol/m^3)	C_{CH0} (mol/m^3)
Deionized water	3.4	20.4	22.4	6820.89	3602.87
3% NaCl	8.0	23.6	25.6	6820.89	3602.87

A comparative analysis of these parameters (x_1, x_2, and C_{satu}) shows that the values in 3% NaCl are consistently higher than those in deionized water. This suggests an accelerated dissolution of solid-phase calcium under 3% NaCl attack, likely due to a more significant concentration gradient of calcium ions between the pore solution and the external environment. Additionally, the equilibrium curve in 3% NaCl lies below that in deionized water, implying that for identical calcium ion concentrations in the pore solution, cement pastes in 3% NaCl retain less solid-phase calcium. This observation indicates that calcium leaching in cement pastes is more pronounced under 3% NaCl attack compared to deionized water. When comparing only the saturated concentration of calcium ions, calcium leaching in cement pastes exposed to 3% NaCl accelerated by approximately 14% compared to that in deionized water.

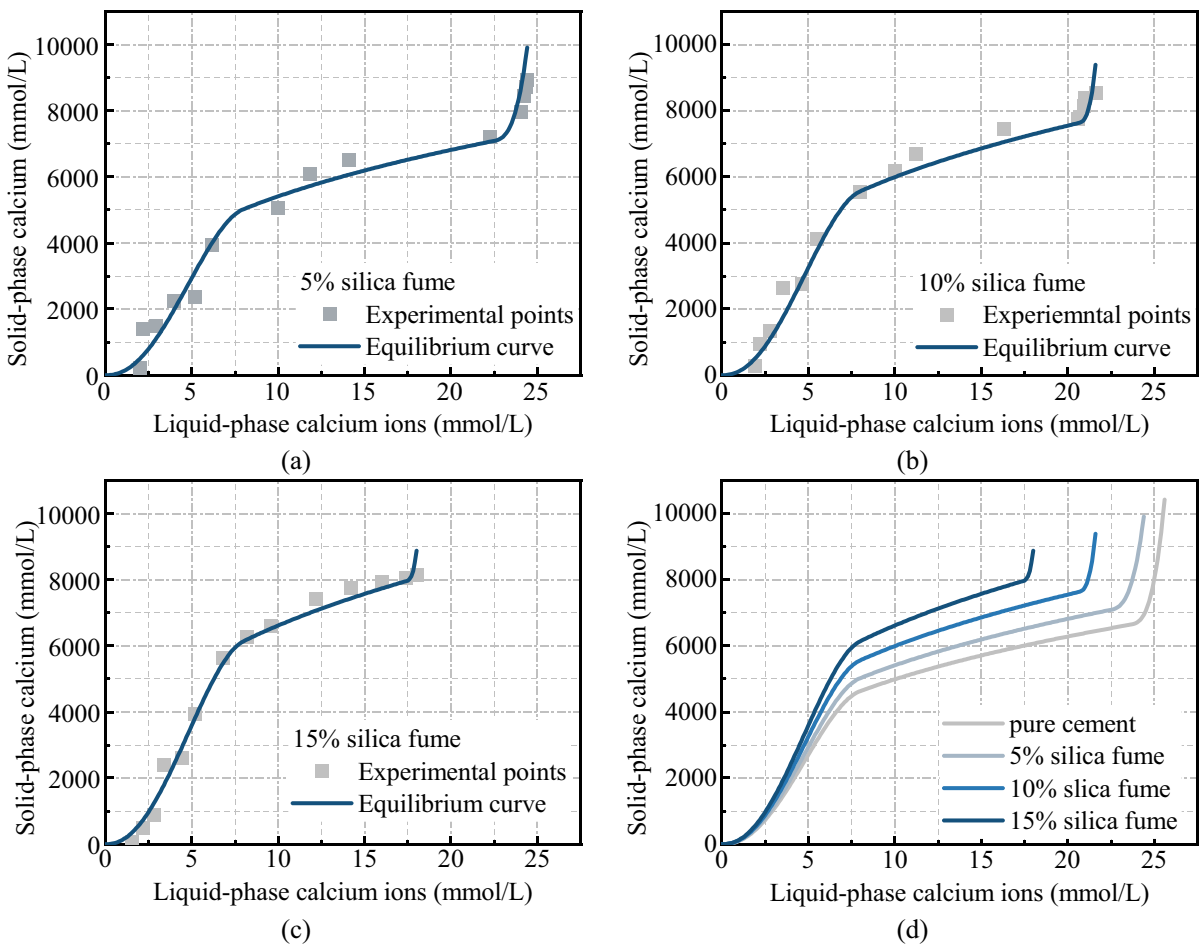

Fig. 3 Solid–liquid equilibrium curves of silica fume–cement pastes: **a** 5% silica fume, **b** 10% silica fume, **c** 15% silica fume, **d** comparison of equilibrium curves

Table 5 Fitting parameters of equilibrium curves in the silica fume–cement paste group

Silica fume-content (%)	x_1 (mol/m^3)	x_2 mol/m^3)	C_{satu} (mol/m^3)	C_{CSH0} (mol/m^3)	C_{CH0} (mol/m^3)
0	8.0	23.6	25.6	6820.89	3602.87
5	8.0	22.4	24.4	7282.68	2625.74
10	8.0	20.6	21.6	7745.04	1646.64
15	8.0	17.4	18.0	8046.02	827.54

3.1.2 Solid–liquid equilibrium curves of silica fume–cement pastes in 3% NaCl

Figure 3 illustrates the solid–liquid equilibrium curves for silica fume–cement pastes in a 3% NaCl solution. These curves, representing silica fume proportions of 5, 10, and 15%, all exhibit a three-stage leaching behavior. The experimental data fit well with the classical solid–liquid equilibrium equation. Key parameters of the equilibrium curve are summarized in Table 5. As the silica fume dosage increases, the saturated calcium concentration (C_{satu}) and the liquid-phase calcium concentration at the onset of slow C–S–H leaching (x_2) show a decreasing trend, while the liquid-phase calcium concentration at the onset of rapid C–S–H leaching (x_1) remains constant at 8 mmol/L. Calcium leaching in cementitious materials involves two primary processes: dissolution and diffusion transport of ions. The lower ion concentrations (x_1, x_2, and C_{satu}) in the pore solution, as observed with increasing silica fume content, contribute to a reduced concentration gradient. This reduction in gradient during the outward diffusion of calcium ions consequently decelerates the dissolution process [40].

The dissolution stage of CH in the composite binder paste shortens with increasing silica fume dosage. This is attributed to the reduced cement content in the composite binder pastes and the consumption of CH by the high silica content in the replacement material [60]. Silica fume, with a high SiO_2 content of 96.8%, reacts with CH in cement hydrates to form C–S–H gel. In silica fume–cement composite pastes, the CH content decreases due to cement replacement, but the overall C–S–H content increases owing to secondary hydration. The resultant C–S–H gel reduces porosity, thereby enhancing the material's resistance to leaching [20]. Notably, as depicted in Fig. 3c, when the silica fume content reaches 15%, the CH dissolution stage is almost absent in the equilibrium curve. It is important to control the silica fume proportion in composite cement pastes to avoid the drawbacks of excess silica fume, which may not contribute to secondary hydration effects and can be costly. Optimal amounts of silica fume can significantly improve the dissolution resistance of cementitious materials due to its potent hydration activity.

3.1.3 Solid–liquid equilibrium curves of fly ash–cement pastes in 3% NaCl

Figure 4 shows the solid–liquid equilibrium curves for fly ash–cement pastes in 3% NaCl, focusing on fly ash dosages of 10, 20, and 30%. Similar to previous observations, these curves exhibit a three-stage leaching behavior, with the CH dissolution stage becoming progressively shorter as the fly ash content increases. The classical solid–liquid equilibrium equation fits the experimental data well, and the fitting parameters are summarized in Table 6. Notably, as the fly ash dosage increases, both the saturated calcium concentration (C_{satu}) and the liquid-phase calcium concentration at the onset of slow C–S–H leaching (x_2) decrease, while the liquid-phase calcium concentration at the onset of rapid C–S–H leaching (x_1) consistently remains at 8 mmol/L. This pattern is attributed to the pozzolanic reaction of fly ash, which reduces the concentration of liquid-phase calcium in the pore solution, thereby diminishing the outward diffusion gradient of calcium ions [23].

Fly ash serves two distinct functions in composite binder pastes: (i) as a filler and (ii) as a reactive chemical component [61]. Similar to silica fume–cement pastes, the CH dissolution stage is reduced with increasing fly ash content [52]. At a 30% fly ash content, as illustrated in Fig. 4c, the CH dissolution stage is barely perceptible due to the complete consumption of CH by the secondary hydration of fly ash. However, in comparison to pure cement pastes, the C–S–H content in fly ash–cement composite pastes is

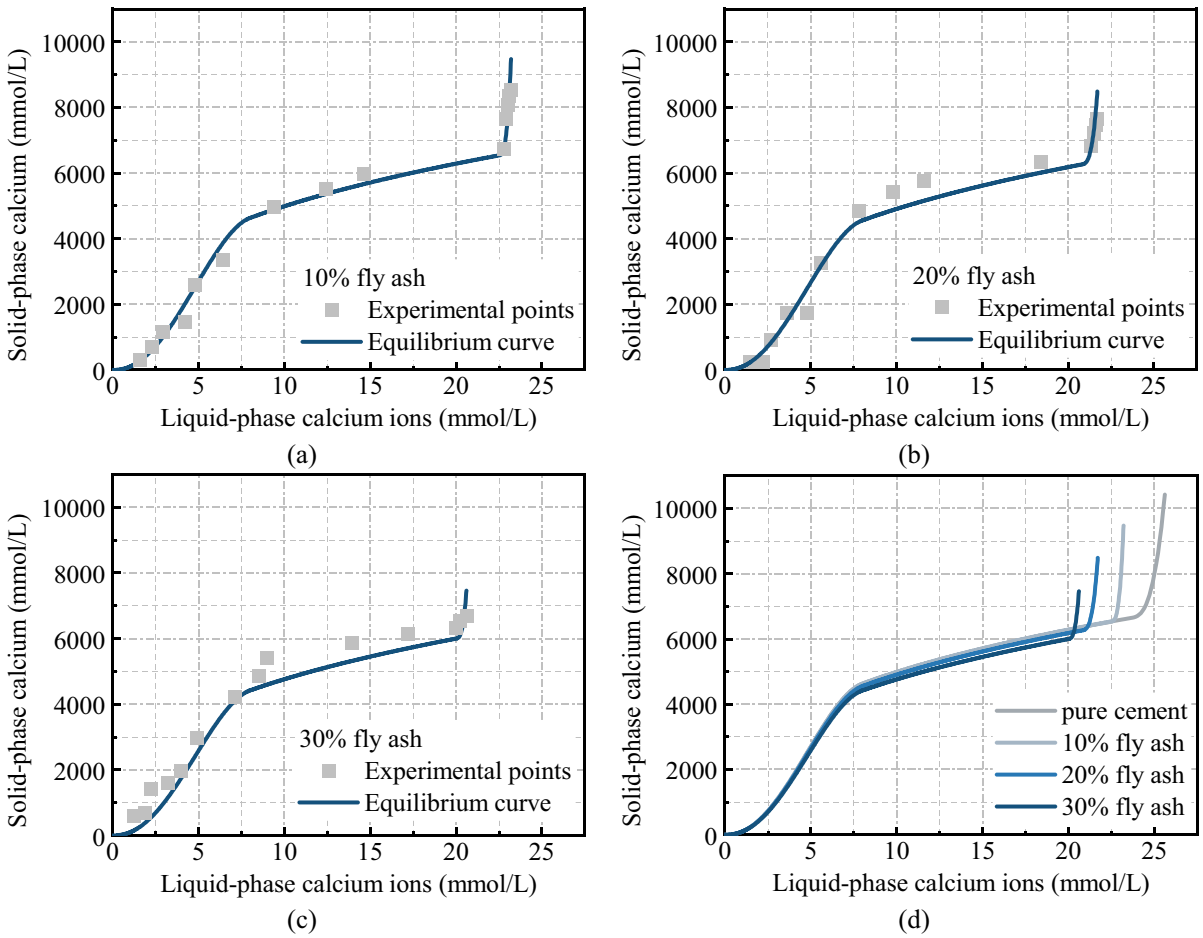

Fig. 4 Solid–liquid equilibrium curves of fly ash–cement pastes: **a** 10% fly ash, **b** 20% fly ash, **c** 30% fly ash, **d** comparison of equilibrium curves

Table 6 Fitting parameters of equilibrium curves in the fly ash–cement paste group

Fly ash content (%)	x_1 (mol/m^3)	x_2 (mol/m^3)	C_{satu} (mol/m^3)	C_{CSH0} (mol/m^3)	C_{CH0} (mol/m^3)
0	8.0	23.6	25.6	6820.89	3602.87
10	8.0	22.5	23.2	6606.51	2863.14
20	8.0	20.8	21.7	6352.24	2128.89
30	8.0	20.0	20.6	6059.74	1399.34

lower, indicating that the secondary hydration effect of fly ash is weaker than that of silica fume [62]. The increase in C–S–H gel content from fly ash hydration does not fully compensate for the reduction caused by the decreased cement content. A significant drawback of adding fly ash is the reduction of early strength in mortars and concrete [63]. Consequently, composite cement pastes containing fly ash exhibit inferior calcium leaching resistance compared to those containing silica fume [64].

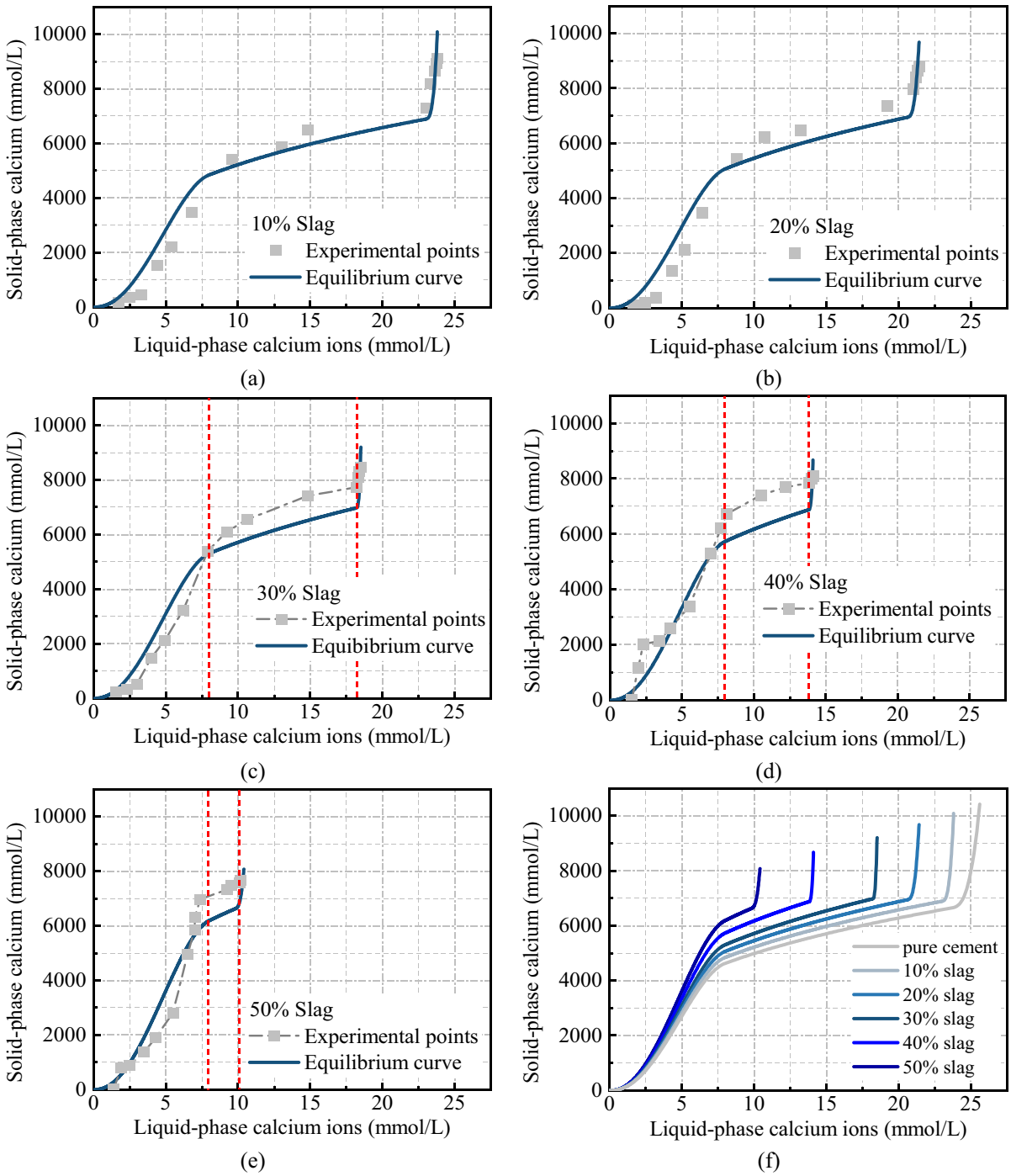

Fig. 5 Solid–liquid equilibrium curves of slag–cement pastes: **a** 10% slag, **b** 20% slag, **c** 30% slag, **d** 40% slag, **e** 50% slag, **f** comparison of equilibrium curves

Table 7 Fitting parameters of equilibrium curves in the slag–cement paste group

Slag content (%)	x_1 (mol/m^3)	x_2 (mol/m^3)	C_{satu} (mol/m^3)	C_{CSH0} (mol/m^3)	C_{CH0} (mol/m^3)
0	8.0	23.6	25.6	6820.89	3602.87
10	8.0	23.0	23.8	6968.68	3119.88
20	8.0	20.6	21.4	7032.14	2646.95
30	8.0	18.2	18.5	7016.83	2186.92
40	8.0	13.8	14.1	6925.17	1743.74
50	8.0	9.8	10.4	6756.65	1322.88

3.1.4 Solid–liquid equilibrium curve of slag–cement pastes in 3% NaCl

Figure 5 displays the solid–liquid equilibrium curves for slag–cement pastes in a 3% NaCl solution. Similar to the effects observed with silica fume and fly ash, the addition of slag maintains the three-stage leaching process of CH and C–S–H. The fitting parameters for these curves are presented in Table 7. With an increasing dosage of slag, both the saturated calcium concentration (C_{satu}) and the liquid-phase calcium concentration at the onset of slow C–S–H leaching (x_2) show a decreasing trend, while the liquid-phase calcium concentration at the onset of rapid C–S–H leaching (x_1) remains constant at 8 mmol/L.

As the proportion of slag is increased, the CH dissolution stage is notably shortened, reflecting the additional calcium demand created by slag hydration. This demand is met either by CH resulting from Portland cement hydration [58] or by a lower C/S ratio in the C–S–H [65]. Additionally, the total concentration of solid-phase calcium decreases with a rising slag dosage. However, the C–(A)–S–H content first increases and then decreases, peaking at a 20% slag proportion. This peak is attributed to the reduction in C–S–H due to lower cement content and the concurrent increase in C–(A)–S–H from slag hydration.

The hydration process of slag–cement pastes is more complex compared to pastes containing silica fume and fly ash, influenced by various factors like water–cement ratio, temperature, slag reactivity, and fineness. Consequently, accurately calculating the initial concentrations of CH and C–S–H (C–A–S–H) through theoretical derivation is challenging [58]. Therefore, an averaged calcium–silicon ratio of C–S–H and C–A–S–H was used for the solid–liquid equilibrium curve, falling between the C/S ratios of C–A–S–H and C–S–H. As shown in Fig. 5, experimental values in the rapid dissolution stage of C–S–H are lower than theoretical values, while in the slow dissolution stage, they are higher.

Despite this, the key focus of this study is the key parameters of liquid-phase calcium, corresponding to the inflection points of the equilibrium curves. The horizontal coordinates of the inflection points in both experimental and theoretical curves align well, as seen in Fig. 5. This alignment indicates that the study successfully captures the crucial aspects of calcium leaching.

3.2 Relationship between key parameters of equilibrium curve and SCM proportion

The solid–liquid equilibrium curve is essential for understanding the relationship between calcium concentration in cement hydrates and pore solutions. It facilitates the calculation of the dissolution rate of solid-phase calcium in the transport-reaction equation of calcium ions. Within this curve, C_{CSH0} and C_{CH0} are derived from the chemical and mineral composition of cementitious materials, while x_1, x_2, and C_{satu} are influenced by the material composition and erosive environment, necessitating experimental data fitting. Section 3.1 establishes that x_1 remains constant at 8 mmol/L in a 3% NaCl solution and does not change with SCM proportions. Therefore, this study focuses on the functional relationship between x_2 and C_{satu} as influenced by SCM content.

3.2.1 Concentration of calcium ions x_2 at the onset of C–S–H slow leaching

X_2 indicates the concentration of calcium ions at the onset of C–S–H slow leaching. Figure 6 depicts the relationship between SCM content and x_2.

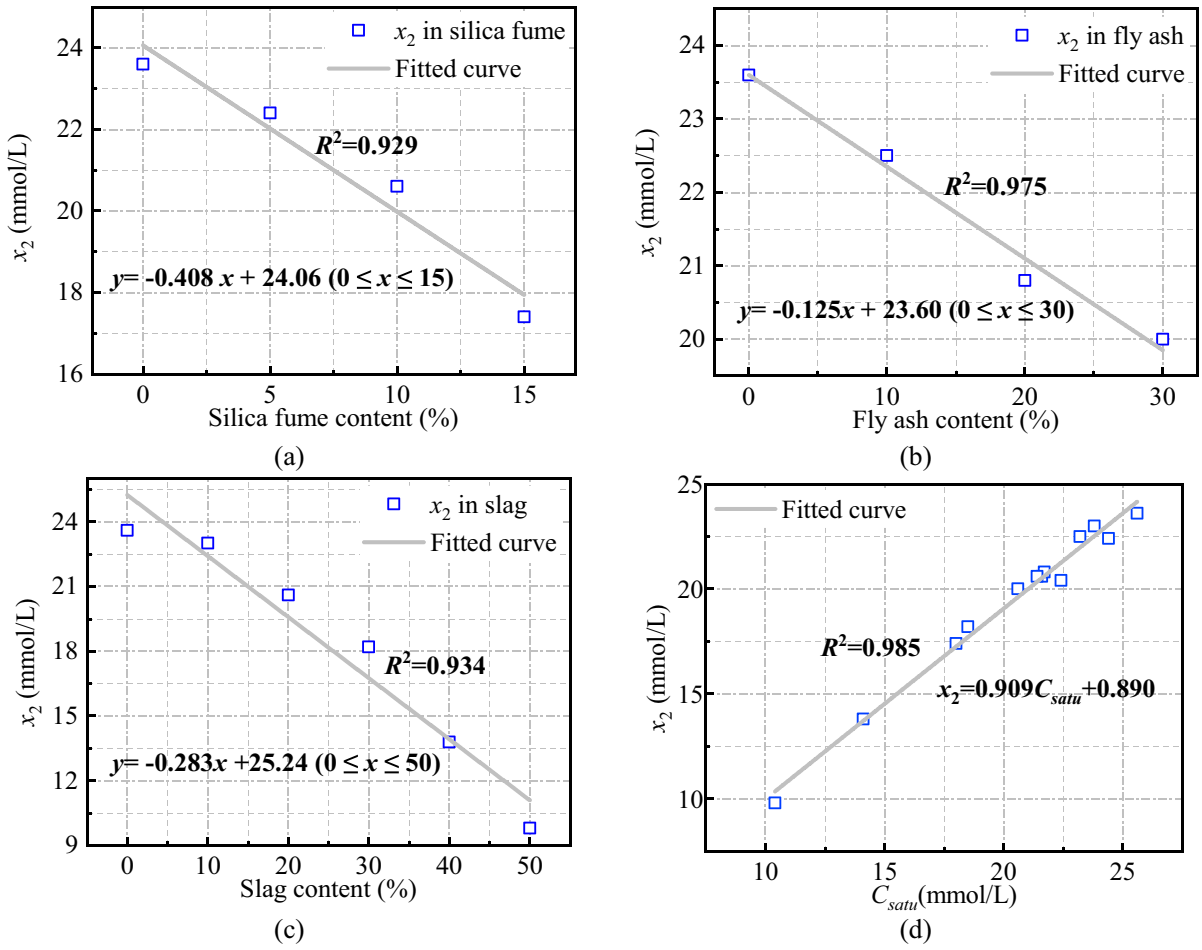

Fig. 6 Critical parameter x_2 for different composite cement pastes: **a** silica fume–cement paste, **b** fly ash–cement paste, **c** slag–cement paste, **d** relationship between C_{satu} and x_2

The fitted curves show a strong linear relationship between SCM content and x_2, with over 90% accuracy, regardless of SCM type. This suggests that with higher SCM proportions within their maximum dosage range, the calcium ion concentration at the start of C–S–H decalcification decreases, which can slow down the C–S–H leaching process by reducing the concentration gradient. Previous studies have used empirical relationships to determine x_2 in relation to the saturated calcium ion concentration [40, 47, 66]. Figure 6d further examines the relationship between x_2 and C_{satu}, revealing a consistent linear relationship with a slope of approximately 90%, aligning with findings reported in [30].

3.2.2 *The saturated concentration of calcium ions in the pore solution*

C_{satu} is a crucial parameter representing the solubility of solid-phase calcium in a 3% NaCl solution. A higher C_{satu} indicates a greater concentration gradient between the pore solution and the external environment, enhancing the dissolution of calcium ions from cement hydrates. While C_{satu} is higher in aggressive solutions compared to deionized water, the addition of SCMs can reduce it. Figure 7 illustrates the relationship between C_{satu} and SCM content. Results show a robust linear correlation between C_{satu} and SCM content, with over 90% accuracy, regardless of SCM type. Figure 7d compares the impact of SCM content on the saturated calcium ions concentration,

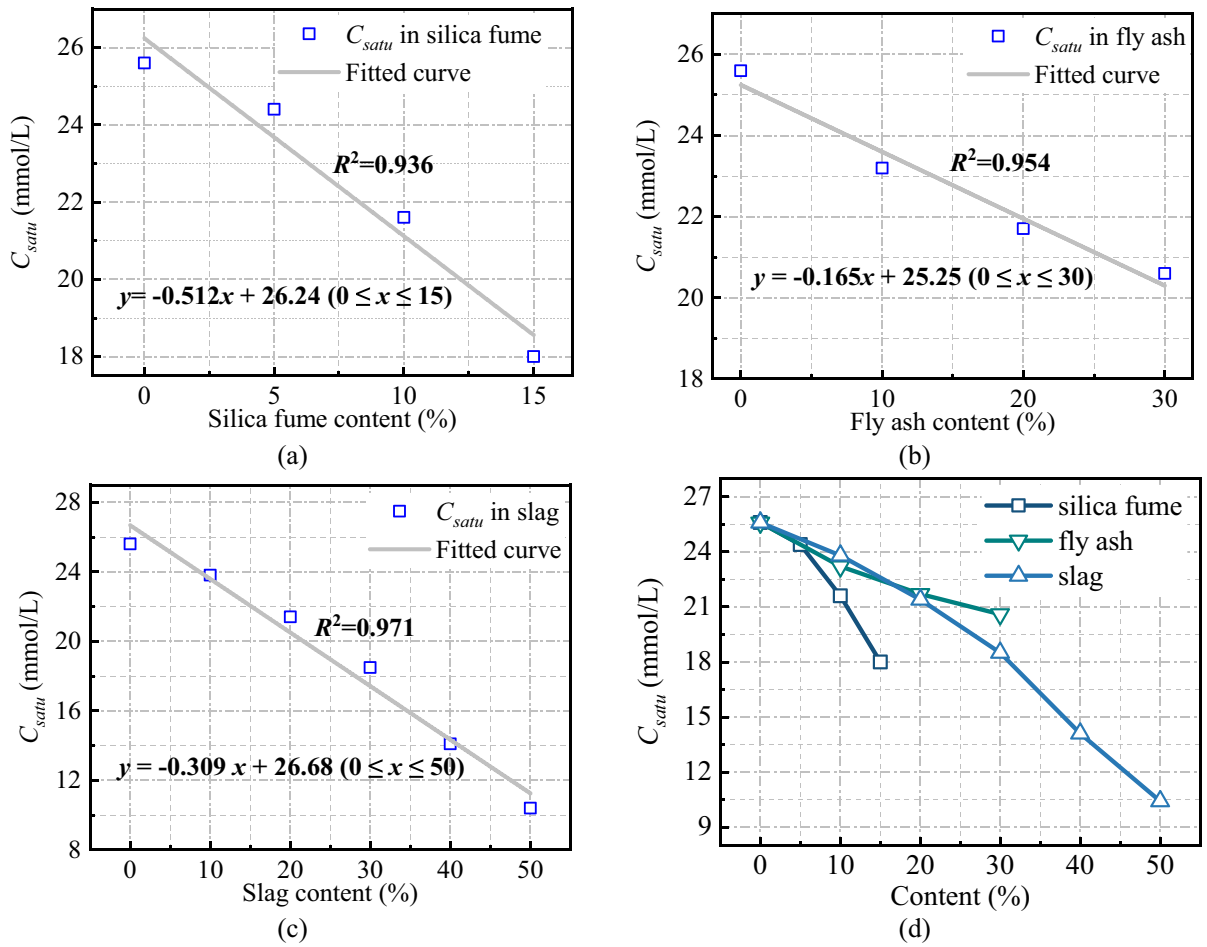

Fig. 7 Critical parameter C_{satu} for different composite cement pastes: **a** silica fume–cement paste, **b** fly ash–cement paste, **c** slag–cement paste, **d** comparison of C_{satu} for different SCM contents

demonstrating that silica fume–cement systems exhibit a more significant decrease in calcium ion saturation for the same SCM proportion change. Hence, controlling silica fume content in composite cement pastes is vital. Within the maximum SCM proportion range, a high slag content can lead to the lowest saturated concentration of calcium ions, potentially enhancing the leaching resistance of cementitious materials.

3.3 Comparison of leaching resistance for different SCM proportions in composite cement pastes

In this section, we compare the leaching resistance of composite cement pastes with varying proportions of SCMs. The solid–liquid equilibrium curve effectively illustrates the calcium leaching stages in cementitious materials, simulating the leaching process under various aggressive conditions and material properties. This curve primarily depicts the decalcification process of cementitious materials at the microscopic pore scale. Therefore, we can only assess the calcium leaching resistance based on solid-phase calcium content and calcium ion concentration gradients.

By analyzing changes in the saturated calcium ions concentration, total calcium concentration, and the relative content of CH and C–S–H, the leachability of different composite cement pastes is compared. The saturated calcium ion concentration in the pore solution reflects the maximum concentration gradient for the outward diffusion of calcium ions. A larger gradient facilitates more calcium dissolution from cement

Table 8 Comparison of leaching resistance performance of composite binder pastes with different SCMs (The experimental group of SL-50 has the best leaching resistance)

ID	R_{csatu}	$R_{CH/CSH}$	R_{Total}	Score
SF-5	0.953	0.683	1.052	2.688
SF-10	0.844	0.403	1.110	2.356
SF-15	0.703	0.195	1.175	2.073
FA-10	0.906	0.82	1.101	2.827
FA-20	0.848	0.634	1.229	2.711
FA-30	0.805	0.437	1.397	2.639
SL-10	0.93	0.848	1.033	2.81
SL-20	0.836	0.713	1.077	2.625
SL-30	0.723	0.590	1.133	2.445
SL-40	0.551	0.477	1.202	2.230
SL-50	0.406	0.371	1.290	2.067

hydrates, implying that pastes with higher leaching resistance have lower saturated calcium ion concentrations. The total calcium concentration, indicative of CH and C–S–H content before leaching, correlates with leaching resistance, with higher total solid-phase calcium suggesting better resistance. Additionally, the C–S–H gel is crucial for cement hydrates, with high C–S–H content generally signifying greater leaching resistance. However, CH is a double-edged sword: while it serves as a reserve for concrete alkalinity, its rapid dissolution can increase porosity and accelerate calcium leaching. Therefore, the ratio of CH to C–S–H is an important indicator of leaching resistance, with lower CH content under the same solid-phase calcium concentration indicating better resistance.

Each composite cement paste was scored for its leaching resistance using Eq. (19), with the results presented in Table 8. R_{csatu} is the ratio of saturated calcium ion concentration in composite binder pastes to that in pure cement pastes. $R_{CH/CSH}$ and R_{total} represent the ratios of calcium phases and total calcium phases in composite binder pastes to those in pure cement pastes, respectively. The experimental condition yielding the lowest Score indicates the best calcium leaching resistance. For silica fume–cement pastes, a 15% silica fume proportion showed the best resistance. For fly ash–cement pastes, a 30% fly ash proportion was optimal. For slag–cement pastes, a 50% slag proportion exhibited the best resistance. A comprehensive comparison reveals that composite cement pastes with 50% slag are the most optimal. These findings align with previous studies by Tang et al. [51], Han et al. [50], and Roziere et al. [67], which conducted accelerated leaching experiments on various composite cement pastes. This concurrence validates the reasonableness and scientific accuracy of this study in assessing leaching resistance from the perspective of solid–liquid equilibrium curves. However, the *Score* is calculated based on equal weighting of the three indicators' impact on leaching resistance performance. The results are semi-quantitative, and further accelerated leaching tests are necessary to validate the study's findings, taking into account various factors such as microstructure, mechanical properties, and phase compositions.

$$\text{Score} = R_{csatu} + R_{CH/CSH} + R_{Total} \tag{19}$$

4 Conclusions

In this study, the solid–liquid equilibrium curves of calcium in composite binder paste exposed to 3% NaCl were investigated. A functional relationship between the key parameters of the leaching curves (x_1, x_2, and C_{satu}) and the proportions of SCMs was established, and the leaching resistance of these pastes was evaluated from the perspective of leaching curves. These findings provide a theoretical foundation for developing concrete deterioration models and guidance for designing anti-leaching concrete. The specific conclusions are as follows:

- The calcium leaching process in NaCl solution followed a similar three-stage pattern as in deionized water. When comparing only the saturated concentration of calcium ions, calcium leaching in cement pastes exposed to 3% NaCl accelerated by approximately 14% compared to that in deionized water.
- In a 3% NaCl environment, both the saturated concentration of calcium ions (C_{satu}) and the liquid-phase calcium concentration at the onset of slow C–S–H leaching (x_2) demonstrated a linear decrease with increasing SCM content, while the liquid-phase calcium concentration at the onset of rapid C–S–H leaching (x_1) consistently remained at 8 mmol/L.

- An analysis of the saturated concentration of calcium ions, the initial total solid-phase calcium content, and the relative content of CH and C–S–H revealed that composite binder pastes with 15% silica fume, 30% fly ash, and 50% slag exhibited enhanced leaching resistance. Notably, silica fume had the most substantial effect on C_{satu}, with 50% slag in the composite cement pastes showing the best overall leaching resistance.

Future research should focus on several key areas: (1) Conducting accelerated leaching experiments in a 3% NaCl solution to validate the optimal SCM proportions; (2) Developing a concrete deterioration model incorporating calcium leaching based on solid–liquid equilibrium curves, and comparing its outcomes with accelerated leaching experiments; (3) Investigating the calcium leaching process in various NaCl concentrations and other aggressive solutions.

Acknowledgements This work was supported by the National Key Research and Development Program of China (Grant No. 2021YFF0500801), the National Natural Science Foundations of China (Grant Nos. 52108234, 52378228), the Guangdong Basic and Applied Basic Research Foundation (Grant No. 2022A1515240031), the National Science Fund for Distinguished Young Scholars of China (Grant No. 52025081), the Shenzhen Science and Technology Program (Grant Nos. RCYX20200714114525013, GXWD20220817143919002, KQTD20210811090112003).

Author's contribution Ming Zhang: Methodology, Writing—original draft, Writing—review & editing, Formal analysis. Peicheng Shen: Validation, Methodology, Investigation. Dujian Zou: Methodology, Conceptualization, Writing—review & editing, Funding acquisition. Tiejun Liu: Supervision, Funding acquisition, Project administration. Shanshan Qin: Writing—review & editing, Funding acquisition. Ao Zhou: Writing—review & editing, Conceptualization. Ye Li: Writing—review & editing, Methodology.

Data availability Data will be made available on request.

Declarations

Conflict of interest The authors declare that there are no conflicts of interests.

References

1. Shi X, Xie N, Fortune K, Gong J (2012) Durability of steel reinforced concrete in chloride environments: an overview. Constr Build Mater 30:125–138
2. Yu Y, Zhang Y (2017) Coupling of chemical kinetics and thermodynamics for simulations of leaching of cement paste in ammonium nitrate solution. Cem Concr Res 95:95–107
3. Choi YS, Yang EI (2013) Effect of calcium leaching on the pore structure, strength, and chloride penetration resistance in concrete specimens. Nucl Eng Des 259:126–136
4. Li X, Zuo X, Zou Y (2021) Modeling and simulation on coupled chloride and calcium diffusion in concrete. Constr Build Mater 271:121557
5. American Concrete Society (2019) ACI 318–19 Building Code Requirements for Structural Concrete. American Concrete Society, Farmington Hills, US
6. The British Standards Institution, BS EN 206:2013 Concrete—Specification, Performance, Production and Conformity, BSI Standard Limited, London, UK, 2014.
7. Ministry of Housing and Urban-Rural Development of the People's Republic of China, GB/T 50476–2008 Standard for Design of Concrete Structure Durability, China Architecture Publishing & Media Co., Ltd., Beijing, China, 2019.
8. Scrivener KL, Nonat A (2011) Hydration of cementitious materials, present and future. Cem Concr Res 41:651–665
9. Rashad AM (2014) A comprehensive overview about the influence of different admixtures and additives on the properties of alkali-activated fly ash. Mater Des 53:1005–1025
10. Taylor R, Richardson I, Brydson R (2010) Composition and microstructure of 20-year-old ordinary Portland cement–ground granulated blast-furnace slag blends containing 0 to 100% slag. Cem Concr Res 40:971–983
11. Zhang W, Shi D, Shen Z, Shao W, Gan L, Yuan Y, Tang P, Zhao S, Chen Y (2023) Reduction of the calcium leaching effect on the physical and mechanical properties of concrete by adding chopped basalt fibers. Constr Build Mater 365:130080
12. Yang H, Monasterio M, Zheng D, Cui H, Tang W, Bao X, Chen X (2021) Effects of nano silica on the properties of cement-based materials: a comprehensive review. Constr Build Mater 282:122715
13. Ren P, Ling T, Mo KH (2022) CO2 pretreatment of municipal solid waste incineration fly ash and its feasible use as supplementary cementitious material. J Hazard Mater 424:127457
14. Goñi S, Frías M, de la Villa RV, Vegas I (2013) Decalcification of activated paper sludge–fly ash-Portland cement blended pastes in pure water. Cement Concr Compos 40:1–6
15. Matte V, Moranville M (1999) Durability of reactive powder composites: influence of silica fume on the leaching properties of very low water/binder pastes. Cement Concr Compos 21:1–9
16. Kim JH, Kim HG, Qudoos A, Ryou J (2019) Effect of leaching on the hardened, microstructural and self-cleaning characteristics of titanium dioxide containing cement mortars. Constr Build Mater 207:640–650
17. Catinaud S, Beaudoin J, Marchand J (2000) Influence of limestone addition on calcium leaching mechanisms in cement-based materials. Cem Concr Res 30:1961–1968

18. Qiao C, Suraneni P, Tsui Chang M, Weiss J (2018) Damage in cement pastes exposed to MgCl2 solutions. Mater Struct 51:1–15.
19. Zuo X, Tang Y, Yin G, Jiang K, He S (2017) Influence of fly ash and its partial replacement by slag on the leaching behavior of blended cement pastes. J Mater Civ Eng 29:04017187
20. Gaitero JJ, Campillo I, Guerrero A (2008) Reduction of the calcium leaching rate of cement paste by addition of silica nanoparticles. Cem Concr Res 38:1112–1118
21. Jiang C, Jiang L, Tang X, Gong J, Chu H (2021) Impact of calcium leaching on mechanical and physical behaviors of high belite cement pastes. Constr Build Mater 286:122983
22. Jiang C, Yu L, Tang X, Chu H, Jiang L (2021) Deterioration process of high belite cement paste exposed to sulfate attack, calcium leaching and the dual actions. J Market Res 15:2982–2992
23. Van Eijk R, Brouwers H (1998) Study of the relation between hydrated Portland cement composition and leaching resistance. Cem Concr Res 28:815–828
24. Phung QT, Maes N, Jacques D, De Schutter G, Ye G (2016) Investigation of the changes in microstructure and transport properties of leached cement pastes accounting for mix composition. Cem Concr Res 79:217–234
25. Zhang W, Zhang M, Hou D (2022) Nanoscale insights into the anti-erosion performance of concrete: a molecular dynamics study. Appl Surf Sci 593:153403
26. Gawin D, Pesavento F, Schrefler BA (2008) Modeling of cementitious materials exposed to isothermal calcium leaching, considering process kinetics and advective water flow. Part 1: Theoretical model. Int J Solids Struct 45:6221–6240.
27. Gawin D, Pesavento F, Schrefler BA (2008) Modeling of cementitious materials exposed to isothermal calcium leaching, considering process kinetics and advective water flow. Part 2: Numerical solution. Int J Solids Struct 45:6241–6268.
28. Mainguy M, Tognazzi C, Torrenti J-M, Adenot F (2000) Modelling of leaching in pure cement paste and mortar. Cem Concr Res 30:83–90
29. Pichler C, Saxer A, Lackner R (2012) Differential-scheme based dissolution/diffusion model for calcium leaching in cement-based materials accounting for mix design and binder composition. Cem Concr Res 42:686–699
30. Zou D, Zhang M, Qin S, Liu T, Tong W, Zhou A, Jivkov A (2022) Calcium leaching from cement hydrates exposed to sodium sulfate solutions. Constr Build Mater 351:128975
31. Qin S, Zou D, Liu T, Jivkov A (2020) A chemo-transport-damage model for concrete under external sulfate attack. Cem Concr Res 132:106048
32. Zou D, Qin S, Liu T, Jivkov A (2021) Experimental and numerical study of the effects of solution concentration and temperature on concrete under external sulfate attack. Cem Concr Res 139:106284
33. Fu Q, Bu M, Li D, Xu W, He J, Niu D (2021) Resistance to sulfate attack and chemo-damage-transport model of sulfate ions for tunnel lining concrete under the action of loading and flowing groundwater.ACS Sustain Chem Eng 9:14307–14326
34. Kuhl D, Bangert F, Meschke G (2004) Coupled chemo-mechanical deterioration of cementitious materials. Part I: Modeling. Int J Solids Struct 41:15–40
35. Nakarai K, Ishida T, Maekawa K (2006) Modeling of calcium leaching from cement hydrates coupled with micropore formation. J Adv Concr Technol 4:395–407
36. Berner U (1992) Evolution of pore water chemistry during degradation of cement in a radioactive waste repository environment. Waste Manage 12:201–219
37. Gerard B, Pijaudier-Cabot G, Laborderie C (1998) Coupled diffusion-damage modelling and the implications on failure due to strain localisation. Int J Solids Struct 35:4107–4120
38. Hidalgo A, Petit S, Domingo C, Alonso C, Andrade C (2007) Microstructural characterization of leaching effects in cement pastes due to neutralisation of their alkaline nature: Part I: Portland cement pastes. Cem Concr Res 37:63–70
39. Wan K, Li Y, Sun W (2013) Experimental and modelling research of the accelerated calcium leaching of cement paste in ammonium nitrate solution. Constr Build Mater 40:832–846
40. Wan K, Li L, Sun W (2013) Solid–liquid equilibrium curve of calcium in 6 mol/L ammonium nitrate solution. Cem Concr Res 53:44–50
41. Tang Y, Yin G, Chen F, Zhang J (2022) Solid–liquid equilibrium state and equation of cement-based materials in ammonium chloride solution. Mater Struct 55:220
42. Yokozeki K, Watanabe K, Sakata N, Otsuki N (2004) Modeling of leaching from cementitious materials used in underground environment. Appl Clay Sci 26:293–308
43. Gawin D, Pesavento F, Schrefler BA (2009) Modeling deterioration of cementitious materials exposed to calcium leaching in non-isothermal conditions. Comput Methods Appl Mech Eng 198:3051–3083
44. Liu X, Feng P, Yu X, Huang J (2022) Decalcification of calcium silicate hydrate (CSH) under aggressive solution attack. Constr Build Mater 342:127988
45. Gérard B, Le Bellego C, Bernard O (2002) Simplified modelling of calcium leaching of concrete in various environments. Mater Struct 35:632–640
46. Phung QT, Maes N, Jacques D, Perko J, De Schutter G, Ye G (2016) Modelling the evolution of microstructure and transport properties of cement pastes under conditions of accelerated leaching. Constr Build Mater 115:179–192
47. Jain J, Neithalath N (2009) Analysis of calcium leaching behavior of plain and modified cement pastes in pure water. Cement Concr Compos 31:176–185
48. Wang Y, Yuan Q, Deng D (2018) Modelling calcium leaching kinetics of cement asphalt paste. Mater Struct 51:1–13
49. Chen T, Li L, Gao X, Guo M, Qin L (2023) New insights into the role of early accelerated carbonation on the calcium leaching behavior of cement paste. Cement Concr Compos 140:105103
50. Han F, Liu R, Yan P (2014) Effect of fresh water leaching on the microstructure of hardened composite binder pastes. Constr Build Mater 68:630–636
51. Tang Y, Zuo X, He S, Ayinde O, Yin G (2016) Influence of slag content and water-binder ratio on leaching behavior of cement pastes. Constr Build Mater 129:61–69

52. Cai X, He Z, Shao Y, Sun H (2016) Macro-and micro-characteristics of cement binders containing high volume fly ash subject to electrochemical accelerated leaching. Constr Build Mater 116:25–35
53. ASTM D1141–98. Standard practice for the preparation of substitute ocean water[J]. American Society for Testing and Materials, USA, 1998.
54. Yu C, Wu Q, Yang J (2017) Effect of seawater for mixing on properties of potassium magnesium phosphate cement paste. Constr Build Mater 155:217–227
55. Ganjian E, Pouya HS (2005) Effect of magnesium and sulfate ions on durability of silica fume blended mixes exposed to the seawater tidal zone. Cem Concr Res 35:1332–1343
56. De Weerdt K, Lothenbach B, Geiker MR (2019) Comparing chloride ingress from seawater and NaCl solution in Portland cement mortar. Cem Concr Res 115:80–89
57. Kim J, Vipulanandan C (2003) Effect of pH, sulfate and sodium on the EDTA titration of calcium. Cem Concr Res 33:621–627
58. Chen W, Brouwers H (2007) The hydration of slag, part 2: reaction models for blended cement. J Mater Sci 42:444–464
59. Bentz DP, Jensen OM, Coats A, Glasser FP (2000) Influence of silica fume on diffusivity in cement-based materials: I. Experimental and computer modeling studies on cement pastes. Cem Concr Res 30:953–962
60. Jain J, Neithalath N (2009) Physico-chemical changes in nano-silica and silica fume modified cement pastes in response to leaching. Int J Mater Struct Integrity 3:114–133
61. Gartner E (2004) Industrially interesting approaches to "low-CO2" cements. Cem Concr Res 34:1489–1498
62. Singh N, Kalra M, Kumar M, Rai S (2015) Hydration of ternary cementitious system: Portland cement, fly ash and silica fume. J Therm Anal Calorim 119:381–389
63. Barbhuiya S, Gbagbo J, Russell M, Basheer P (2009) Properties of fly ash concrete modified with hydrated lime and silica fume. Constr Build Mater 23:3233–3239
64. Suarez L, Abu-Lebdeh TM, Picornell M, Hamoush SA (2016) Investigating the role of fly ash and silica fume in the cement hydration process. Am J Eng Applied Sci 9:134–145
65. Kolani B, Buffo-Lacarrière L, Sellier A, Escadeillas G, Boutillon L, Linger L (2012) Hydration of slag-blended cements. Cement Concr Compos 34:1009–1018
66. Bejaoui S, Bary B (2007) Modeling of the link between microstructure and effective diffusivity of cement pastes using a simplified composite model. Cem Concr Res 37:469–480
67. Roziere E, Loukili A (2011) Performance-based assessment of concrete resistance to leaching. Cement Concr Compos 33:451–456

Publisher's Note Springer Nature remains neutral with regard to jurisdictional claims in published maps and institutional affiliations.

Springer Nature or its licensor (e.g. a society or other partner) holds exclusive rights to this article under a publishing agreement with the author(s) or other rightsholder(s); author self-archiving of the accepted manuscript version of this article is solely governed by the terms of such publishing agreement and applicable law.